Edge-Light

Exploiting Luminescent Solar Concentrators for Ambient Light Communication

Chávez Tapia, Miguel A.; Rodríguez, Diego Palma; Zamalloa, Marco Zúñiga

DOI
10.1145/3678574

Publication date
2024

Document Version
Final published version

Published in
Proceedings of the ACM on Interactive, Mobile, Wearable and Ubiquitous Technologies

Citation (APA)
Chávez Tapia, M. A., Rodríguez, D. P., & Zamalloa, M. Z. (2024). Edge-Light: Exploiting Luminescent Solar Concentrators for Ambient Light Communication. *Proceedings of the ACM on Interactive, Mobile, Wearable and Ubiquitous Technologies*, *8*(3), Article ART94. https://doi.org/10.1145/3678574

Edge-Light: Exploiting Luminescent Solar Concentrators for Ambient Light Communication

MIGUEL A. CHÁVEZ TAPIA*, Delft University of Technology, The Netherlands
DIEGO PALMA RODRÍGUEZ, Universidad de Ingeniería y Tecnología - UTEC, Perú
MARCO ZÚÑIGA ZAMALLOA, Delft University of Technology, The Netherlands

A recent advance in embedded Internet of Things (IoT) exploits ambient light for wireless communication. This new paradigm enables highly efficient links via simple light modulation, but the design space has a fundamental constraint: *in most State of the Art (SoA) studies, the link can **only** follow the propagation direction of ambient light.* Consider, for example, a swarm of drones and ground robots that want to communicate with sunlight. Drone-to-robot communication could be possible because sunlight travels downwards from the air (drone) to the ground (robot), allowing drones to modulate light to send information to robots beneath them. Robot-to-robot communication, however, is not possible because sunlight does not travel sideways (parallel to the ground). To allow *'lateral communication'* with ambient light, we propose using Luminescent Solar Concentrators (LSC). These optical components receive ambient light on their surface and re-direct part of the spectra towards their edges. Considering this optical property of LSC, our work has three main contributions. First, we benchmark various optical properties of LSC to assess their performance for ambient light communication. Second, we combine LSC with liquid crystal (LC) shutters to form lateral links with ambient light. Third, we test our links indoors and outdoors with artificial and natural ambient light, by enhancing two robots with our LSC transceivers and showing that they can exchange basic commands and coordinate tasks by communicating only with sunlight.

CCS Concepts: • **Hardware** → **Wireless devices**; • **Networks** → **Physical links**.

Additional Key Words and Phrases: visible light communication, passive visible light communication, robot-to-robot communication, sunlight communication

ACM Reference Format:
Miguel A. Chávez Tapia, Diego Palma Rodríguez, and Marco Zúñiga Zamalloa. 2024. Edge-Light: Exploiting Luminescent Solar Concentrators for Ambient Light Communication. *Proc. ACM Interact. Mob. Wearable Ubiquitous Technol.* 8, 3, Article 94 (September 2024), 23 pages. https://doi.org/10.1145/3678574

1 Introduction

In recent years there has been an increasing interest in visible light communications (VLC) as a complement to traditional radio wireless communications. VLC systems leverage the *free light spectrum* to create optical links and can be divided into two main sub-domains: active and passive. In active VLC, the transmitter modulates *directly* the intensity of LEDs to send information. In passive VLC, most transmitters use liquid crystal (LC) shutters to control the intensity of ambient light [5, 7, 8, 13, 30–32, 34, 35].

*Corresponding author

Authors' Contact Information: Miguel A. Chávez Tapia, Delft University of Technology, Delft, The Netherlands, m.a.chaveztapia@tudelft.nl; Diego Palma Rodríguez, Universidad de Ingeniería y Tecnología - UTEC, Lima, Perú, diego.palma@utec.edu.pe; Marco Zúñiga Zamalloa, Delft University of Technology, Delft, The Netherlands, m.a.zunigazamalloa@tudelft.nl.

ACM 2474-9567/2024/9-ART94
https://doi.org/10.1145/3678574

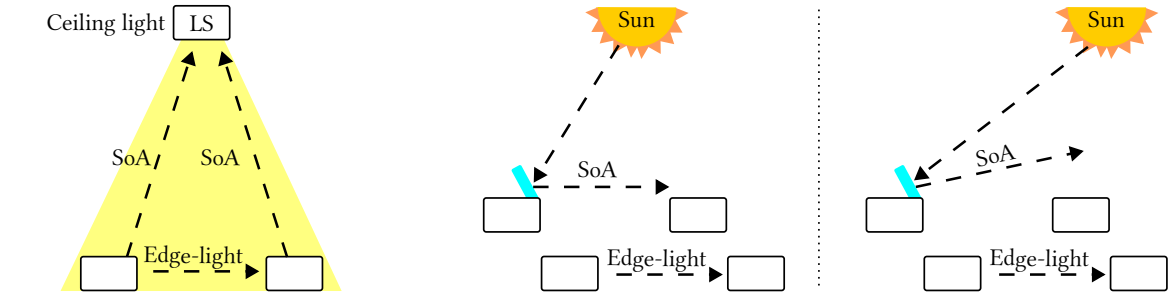

(a) Indoor backscattering Passive VLC. (b) Sunlight Passive VLC.

Fig. 1. Different scenarios comparing Edge-Light to SoA.

The advantage of active VLC is its data rate. Since LEDs can be modulated at faster speeds than LCs, active VLC achieves several hundreds Mbps (or even Gbps) compared to a few Kbps for passive VLC. The advantage of passive VLC is energy efficiency. Passive transmitters do not need to consume energy to generate light, the optical beam is obtained directly from ambient light. This advantage allows passive VLC to consume less than one micro-joule per bit [34], while active VLC with similar ranges consumes 30× more energy per bit [9].

Challenge: link rigidity. Passive VLC is a promising technology for low-end embedded applications but has shortcomings. One of those limitations is the inability to modify the link's direction. Contrary to radio systems, whose antenna arrays can determine the beam direction, passive VLC has *no control* over the light source. This lack of control implies that the communication direction is fixed: the link can *only* follow the same propagation direction of ambient light. Consider the scenario in Figure 1a, where objects in different areas report information to the light source using existing backscattering methods [13, 34]. With current techniques, the objects cannot communicate directly with each other. Placing mirrors on the side could enable lateral communication, but if the objects move the reflection angles change and the links break (Figure 1b). The mirrors would need to be mechanically aligned, increasing the complexity and energy cost of the system. This misalignment issue would be even more critical in scenarios with mobile robots.

Contribution: lateral communication. To expand the link design space of passive VLC, we propose using Luminescent Solar Concentrators (LSC). These optical materials absorb a specific band of light and convert it to a different band (color). LSC also feature wave-guiding properties, the converted band is emitted towards the edges. A typical application of LSC is energy harvesting in windows. The LSC receives sunlight over its surface and redirects part of the spectrum towards the edges (window frame) where solar panels harvest energy arriving from the converted band [20].

A key advantage of LSC is that, independently of the incidence angle of ambient light, it *always* directs spectral energy towards the edge, no mechanical alignment is required. In this work, we analyze the optical properties of LSC and design a novel link to achieve lateral communication with ambient light. Overall, our study, named Edge-Light, provides the following contributions.

Contribution 1: LSC analysis [section 2]. Two central properties of any wireless link are its range and field-of-view (FoV). LSC materials have a limited optical conversion efficiency, around ~5 %[1] or higher for research-based LSC [23, 24]. Due to this low efficiency, the expected strength of the LSC's emitted light is limited. We thoroughly analyze different commercial LSCs to identify the one that provides the best coverage in terms of range and field-of-view.

[1]We measure the *peak intensity* in the absorption band and *peak intensity* in the emission band of one COTS LSC.

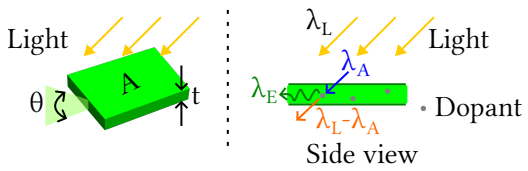

Fig. 2. LSC overview. Area: (A), thickness (t) and field of view (FoV, θ). Dopants molecules absorbe photons (λ_A) in the absorption band and emits photons (λ_E) in the emission band.

Contribution 2: wireless link design and evaluation [section 3]. LSC redirect light but does not modulate it. To build a transmitter, we pair LSC with liquid crystal (LC) shutters and implement frequency-based modulation to cope with the variable intensity of ambient light. To build a receiver, we consider the fact that LSC absorbs white light but emits color light. Thus, we analyze two sensing approaches: color sensors and photodiodes plus color filters. Our final receiver includes various optical components to increase the link's SNR. We perform thorough evaluation of Edge-Light under artificial ceiling lightning and natural sunlight.

Contribution 3: sample application in robot-to-robot communication [section 4]. We build different prototypes of Edge-Light on top of robots and design a protocol for them to exchange three different commands. Our evaluation shows that robots can reliably send these commands (rotate, move forward, stop) for ranges up to one meter. As a sample application, we show a scenario where a single robot cannot move a box, but two robots coordinate and move the box communicating their commands only with sunlight.

2 Luminiscent Solar Concentrator

In essence, an LSC receives light spectra on its surface and emits a different spectrum while guiding it to its edges. To describe the LSC operation we need to define three bands: *incoming*, *absorbing* and *emitted*. Figure 2 shows how these bands interact with each other. First, the incoming band is received over the LSC surface. In our case, the incoming band is white ambient light. Second, internally the LSC transfers spectral energy from an *absorbing band* to an *emitted band*. In Figure 2, the LSC absorbs energy from the blue band and transfers it to the emitted green band. The incoming light does not need to be white and the emitted light can be of different colors. Furthermore, independently of the angle of incidence of ambient light, the LSC always emits light towards the edge. This is an important property to maintain a lateral link when the light source or object moves.

These absorption and emission features stem from the physical structure and properties of two materials constituting an LSC: a host and a dopant. The *host* is, in essence, a waveguide, and its main function is to trap the emitted light by total internal reflection (TIR), guiding this light to its edges. The *dopant* is added to the host and it defines the absorption and emission properties of the LSC. At a molecular level, the dopant absorbs photons from a specific wavelength and then emits a photon in a different wavelength.

The research community has explored various types of materials to manufacture LSC while tuning and improving its response. There are different types of hosts that implement different types of TIR, such as refraction-based [14, 37] or photonic crystal [3, 10]; and different types of dopants, such as organic luminophores or quantum dots (QD) [19, 20], to control not only the LSC's absorption and emission spectra but also its response time. Delving into the details of the various types of LSC is not in the scope of this research, but as this material is a core component of our system, we analyze in this section the properties of commercial of-the-shelve (COTS) LSC. We purchase an assortment of LSCs from Alt® and Pyrasied©, presented in Table 1, and analyze their performance. For these LSCs, the host is acrylic (Polymethylmethacrylate, PMMA) and the dopants are fluorescent dyes.

From a wireless communication perspective, we are interested in analyzing three main LSC parameters. First, the spectral response of the emission band, since color bands represent independent channels in optical communication. Second, the signal-to-noise ratio (SNR) of the emission band, because it determines the link

Manufacturer	Colours	Thickness (mm)
Alt®	Green, Orange	3 mm
Pyrasied©	Blue, Green, Red	8 mm

Table 1. LSC materials

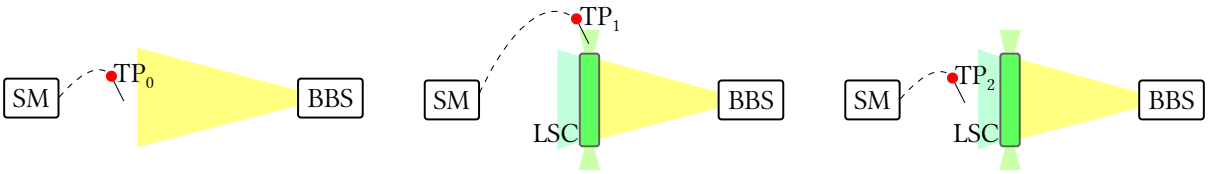

(a) Light emitted by the BBS. (b) Light emitted laterally by LSC. (c) Light passing through the LSC.

Fig. 3. Setup to measure the LSC spectrum. SM: spectrometer, BBS: broadband source. TP: test point.

quality. Third, the response time of the dopant, to guarantee that no delays are introduced in the modulation process.

2.1 Spectral response

The spectral response of the LSC is defined by the absorption band and the emission band. Considering that LSCs have different spectral responses, the research questions we need to answer are: *What LSCs are better suited for passive communication? Which emission bands provide the stronger signals? Which emission bands could be combined to provide multiple input channels?* To answer these questions, we provide a thorough analysis of the absorption and emission bands of the four different colors of LSC[2]. However, since most COTS LSCs are sold without information regarding their spectral response, we must empirically determine it.

Setup. To measure the light spectra of the LSCs, we use a spectrometer and a broadband light source (BBS). The first step is to get the spectrum of the BBS as a reference, which is the test point 0 (TP_0 in Figure 3a). Second, to measure the emission band, we illuminate each LSC with the BBS and place the spectrometer on the edge of the LSC (TP_1 in Figure 3b). Finally, as it is not possible to measure the absorption band directly, we next place the spectrometer behind the LSC to determine the spectrum that passes through it (TP_2 in Figure 3c) and estimate the absorption band using Equation 1, where S represents a scaling function to normalize the output from 0 to 1.

$$AB = S(TP_0 - TP_2) \tag{1}$$

Results. Figure 4 shows the measured and estimated spectra for each LSC. The shaded gray curves capture the *incoming band* spectrum from the BBS, which provides similar intensities for all bands in the visible spectrum. The black curves represent the estimated *absorption bands*, which are normalized.

The measured *emission band* is presented as a colored line corresponding to each LSC and normalized based on the highest spectral peak of all emission bands (orange in our case). The results show that the red and orange LSCs provide stronger intensities, while the blue LSC provides a weak emission. This occurs because the optical energy within the absorption band is transferred to the emission band. Since the red and orange LSCs have broad absorption bands (black curves), they provide more energy to their emission bands compared to the blue LSC, which has a narrow absorption band.

[2]Blue, Green and Red from Pyrasied©. Orange from Alt®

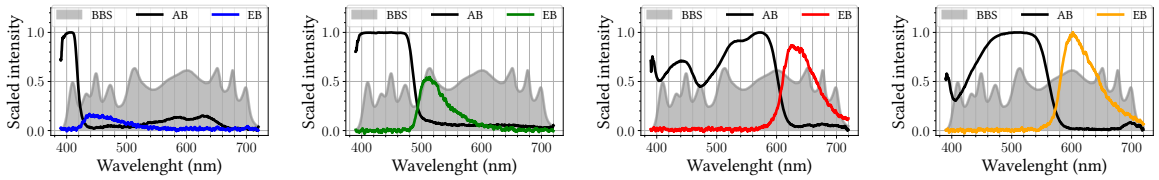

(a) Blue LSC (b) Green LSC (c) Red LSC (d) Orange LSC

Fig. 4. Spectral response of the LSCs. BBS: broadband light source, AB: Absorption band, EB: Emission band.

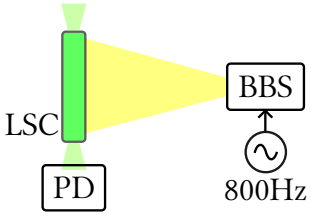

Fig. 5. LSC SNR and response time measurement setup. PD: photodiode.

The red and orange LSCs, however, have overlapping bands, which would cause interference if they are used simultaneously in a network. The green and red LSCs, on the other hand, could provide independent channels. Due to this reason, we consider the green and red LSCs in our evaluation.

2.2 Signal-to-noise ratio

In the prior subsection, we analyzed the effect of the *dopant*. We measured the strength of the emission band, which is dictated by the chemical properties of the dopant. In this subsection, we analyze the effect of the *host*. In particular, the impact that the host's size has on link quality.

Intuitively, a bigger LSC should emit more energy. As shown in Figure 2, a larger area (A_i) would allow capturing more light, and a bigger volume ($A_i \times t_i$) means that more dopants could interact with the incoming light in the absorption band. Therefore, the light emitted by a larger and thicker LSC is expected to be stronger than a smaller and thinner one.

To demonstrate the effect of the LSC's size on the signal strength, we select similar LSC materials but with different areas and thicknesses. Using the setup in Figure 5 and a set of LSC with emission band in the green spectrum, we illuminate the LSC sample with a light source that is oscillating at a frequency of 800 Hz. We place the setup in a dark room and a photodiode (PD), located at 10 cm from the LSC sample, captures the signal emitted by the edge of the LSC. We compute the SNR by calculating the power spectral density (PSD), based on the Fast Fourier Transform (FFT), and comparing the signal's spectral power vs. the noise spectral power. The results in Table 2 show that the area plays a dominant role in increasing the SNR, but the thickness does not. Thus, in our implementation, we try to maximize the area of our transmitter.

2.3 Response time

In the prior section, we saw that a bigger host increases the SNR, but the host is also a waveguide: it steers the emitted light to the LSC edges. And, an important parameter of a waveguide is its response time, which depends on its material and dimensions. In general terms, a thicker waveguide has a slower response time. However, for an LSC an extra factor, related to the dopants, affects the response time.

Dimensions (cm×cm)	Thickness (mm)	SNR (db)
4 × 4	3	1.89
9.6 × 7.6	3	3.48
9.6 × 7.6	8	3.72

Table 2. SNR for different sizes of green-emitting LSCs

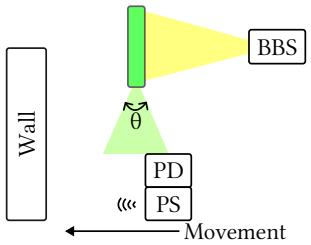

Fig. 6. Setup for measuring LSC output FoV. PS: proximity sensor.

LSCs have been found to have fast responses (in the order of MHz) [20]. The primary reason for this is related to a dopant parameter called *fluorescent lifetime* which can be as short as nanoseconds [22, 25]. This parameter is related to the speed of the dopants reacting to the incoming photons in the absorption band, it means that a higher speed will increase the response of the LSC. In the next section, we propose using liquid crystal shutters as light modulators, and their switching speeds are an order of magnitude slower than the response time of the LSC. Thus, the response time of LSCs is significantly higher than needed for our platform, making LCSs a suitable choice for our purposes.

3 Wireless link design

Our aim is to create a wireless link using the LSC based on the properties we analysed previously: its ability to absorb light in a wide angle of incidence and re-emit it in a different direction (to its edges); and its ability to absorb and emit specific optical bands of the light spectrum. In this section, we present first the design of the transmitter and next the design of the receiver.

3.1 Transmitter

In this section, we first characterize the field-of-view, then we propose a method to increase the signal strength, and conclude with the description of the modulation.

3.1.1 Estimating the field of view. An important parameter in wireless communication is the field of view FoV of the transmitter, which is the angle θ in Figure 2. Since the LSC is a waveguide, the field of view (also called numerical aperture), depends on the refractive index of the waveguide material. The host material is PMMA (acrylic), the same material as plastic optical fibres (POF), thus it is expected they have a similar FoV of ±30°.

We use the setup in Figure 6 to measure the FoV of two green-emitting LSC samples with different widths, 8 mm and 3 mm. The setup uses an ultrasound proximity sensor (PS) attached to the PD to measure the distance relative to a reference point[3]. The results presented in Figure 7, normalized to the maximum intensity, show that the FoV is the same as optical fibers, ±30° and the width has little effect on the coverage.

[3]The FoV of the PD is larger than the LSC

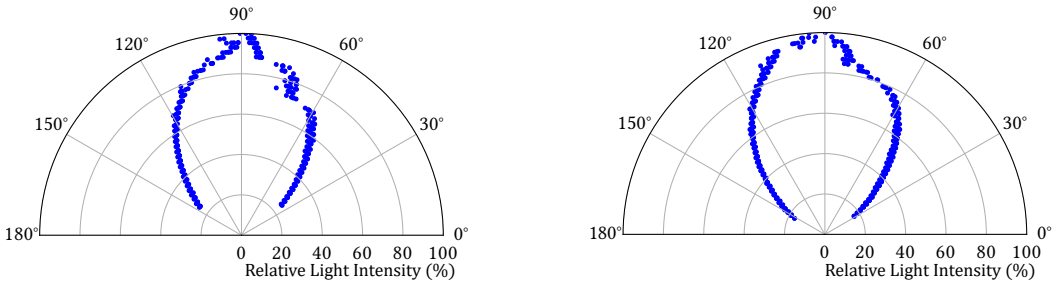

(a) 3 mm green-emitting LSC sample.

(b) 8 mm green-emitting LSC sample.

Fig. 7. FoV for two LSC samples of the same material but different width. Distance between PD and LSC is 36 mm.

Dimensions (cm×cm)	Thickness (mm)	$SNR_{old} \rightarrow SNR_{new}$
4×4	3	1.89 dB → 2.40 dB
9.6×7.6	3	3.48 dB → 3.73 dB
9.6×7.6	8	3.72 dB → 4.03 dB

Table 3. Boost in SNR by the use of a retro-reflective surface.

3.1.2 Increasing the signal strength. The working principle of the LSC is stochastic: there is a probability (P_A) that a photon in the absorption band triggers a photon in the emission band. A direct way to increase this interaction is to add a reflector under the LSC, thus the photons that are not absorbed by the LSC are forced to pass through it one more time, increasing the chances for them to interact with the dopants and emit more light in the emission band. To test this principle, we place the three LSC samples of different dimensions over a retro-reflective (RR) surface and use the setup on Figure 5 to measure the increase in signal strength. The results in Table 3 show an increase of 0.3 dB. Since the RR surface does not add much overhead, it is thin and light, we use this tape for the remainder of the paper. A mirror could be used instead of the RR tape, but mirrors are heavier and more brittle.

3.1.3 Modulation with Liquid Crystals (LCs). LSC redirects light but does not modulate it. To modulate information, we build on top of the area of ambient light backscattering [13, 34], which uses liquid crystal (LC) shutters to control light intensity. An LC's working principle is based on polarisation changes controlled by voltage: it blocks light when its pins are driven by a voltage above a threshold (dark state), and it allows light to pass through when its pins are driven by a voltage below a threshold (transparent state). LCs are efficient devices that consume sub-microwatt power, but they have a slow switching speed, which limits the data rate. In our sample application, we send simple commands between robots, and hence, the data rate is not a major disadvantage.

Our final transmitter design, presented in Figure 8, consists of three layers, from top to bottom: an LC, an LSC and an RR tape. For the modulation method, we use Frequency Shift Keying (FSK) due to its resilience to ambient light noise [5]. To generate pseudo-sinusoidal carriers, a micro-controller (Arduino Due) drives the LC input voltage at different speeds between 0 V and 3.3 V to oscillate between the blocking and transparent states.

The commands for our application are encoded as symbols in different carrier frequencies. We use a total of three commands (symbol frequencies) as shown in Table 4 in the *'Frequency (TX)'* column. The column *'FFT Frequency (Rx)'* is used at the receiver side and is explained in the next section. In subsection 3.3, we delve into more details about these symbol's frequency selection.

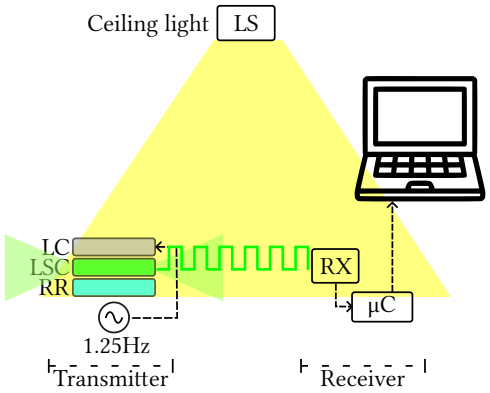

Fig. 8. Setup for testing the receivers under a controlled scenario. μC: microcontroller.

Symbol	Frequency (Tx)	FFT Frequency (Rx)
S_1	5.0 Hz	5.0 Hz
S_2	6.67 Hz	6.25 Hz
S_3	10.0 Hz	10.0 Hz

Table 4. Frequencies for each symbol, based on a 25 ms timer.

3.2 Receiver

The receiver design considers two main points, reducing the noise level (increase the SNR) and selecting the best photosensor to decode the color channels. Depending on the system, SNR levels require a minimum for succesful operation. LoRa requires a minimum of 0 dB but the SNR can be as low as −20 dB depending on the *spread factor* [1]. For a good WiFi connection the lowest SNR is 25 dB. For our system, we determine an empirical threshold for the SNR of ∼5 dB for the link to work with a high success rate, from our results in section 4.

3.2.1 Noise reduction. In free-space optical communication, it is not only important to assess the FoV of the transmitter, which impacts coverage, but also the FoV of the receiver because it affects the SNR. Ideally, the receiver's FoV should focus *only* on the edge of the LSC because that is the only surface that transmits the signal (S). The space above and below the edge consist of ambient light noise (N). At short ranges, the receiver's FoV covers mainly the LSC edge (high SNR), but as the range increases, the LSC's edge covers only a small part of the receiver's FoV (low SNR).

To cope with ambient noise, a common practice in optical systems is adding a lens in front of the photosensor to focus on the transmitter area. Since the LSC emits the modulated signal on its edge, which has a width in the order of mm, and the strongest light is emitted at the middle point of its width, reducing the FoV allows increasing the signal strength. To keep a lightweight implementation we select a small 9 mm ball lens[4] surrounded by a cap to limit the amount of ambient light further reaching the surface of the optical sensor.

Figure 10 shows the final design of the receiver which we manufacture using a 3D-printing process. This design enhances the SNR, and thus, the range of our link as depicted in Figure 9, where the signal strength is increased by a factor greater than 3×.

[4]Ball lens: 9 mm, K9 glass, Back focal length: ∼2 mm

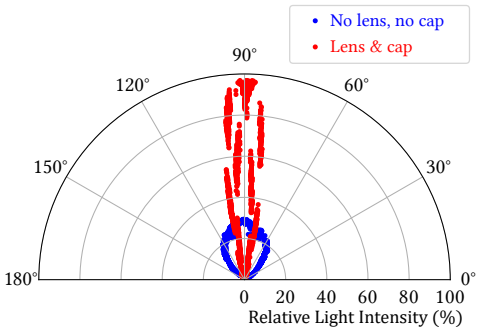

Fig. 9. Effect of the lens on the receiver: FoV reduction and range increase. Distance between PD and LSC is 76 mm.

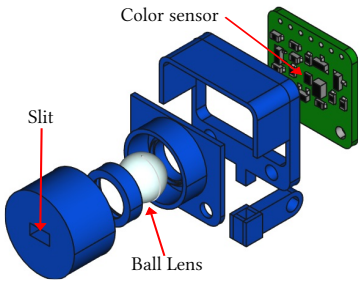

Fig. 10. Final receiver physical design, including a lens, covers and a small slit.

Type	Sensor	Supplier	Angular range[1]	Response time
Light sensor	DFR0026[2]	DFRobot	±45°	15 µs
Phototransistor	TEPT4400	Vishay	±30°	~15 µs
Color sensor	TCS34725	Adafruit	±55°	Variable

Table 5. Types of devices used in the receiver design.
1: Angle of half sensitivity.
2: Based on the PT550 phototransistor.

3.2.2 Sensor selection. For the receiver, we consider the three sensors presented in Table 5: one ambient light sensor, a phototransistor (PT) with tunable gain, and a colour sensor (CS). Color sensors are slow and provide a programmable gain and response time. The response time is determined by the *integration time*, which is the exposure period of the sensor to control its sensitivity. The color sensor has a trade-off: a large integration time renders a higher sensitivity at the cost of increasing the reading time. To attain the fastest possible link, we use the two fastest integration times available for the color sensor, which are 2.4 ms and 24 ms. Moreover, the color sensor features 4 channels: a *clear channel*, which works similar to a photodiode measuring the intensity based on the whole spectrum, and 3 RGB color channels, which measure the intensity of the spectrum corresponding to red, green or blue colors.

The selection criteria for the sensor is the performance under ambient light conditions, using the setup in Figure 8 with the transmitter sending a constant pulse at 1.25 Hz (as in Figure 5). Using the SNR as a metric, and testing for different distances, we analyze three configurations:

- Bare ambient light sensor.
- PT, varying gain according to range.
- CS, reading the *clear channel*.

The results in Figure 11a show that the color sensor at the slowest speed outperforms the other sensors, which is an expected result since the higher exposure time to light allows a stronger signal at the cost of a slower sampling rate. A slow sampling rate is, in general, a shortcoming, but in our design it is not because the LC modulators are slow to begin with.

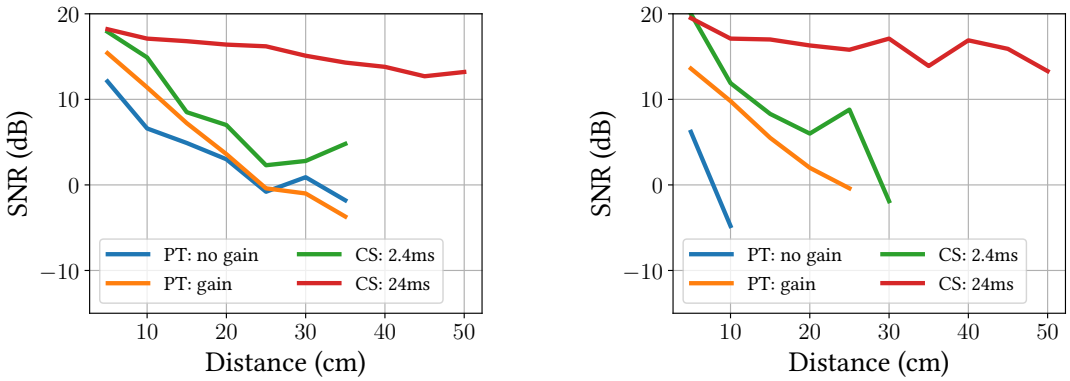

(a) Receivers with no color filter.

(b) Receivers with color filter.

Fig. 11. SNR for different receivers using the same transmitter.

Color filtering dimension. Due to the intrinsic ability of the LSC to absorb and emit different spectrum bands, a further step into the receiver design is assessing its ability to discern different colors. This ability could enable multiple channels to work simultaneously with little interference. To test color filtering, we modify the setup for each sensor:

- Ambient light sensor with a green glass filter.
- PT with a green glass filter.
- CS, reading the green channel.

Using these setups, we note a degradation of all receivers except for the color sensor with a 24 ms sampling rate, as shown in Figure 11b. Given that the color sensor with a sampling rate of 24 ms provides the best SNR with three color channels, we use that photosensor in our system.

3.2.3 Demodulation. To decode the information, we use the Fast Fourier Transform (FFT) implementation on the Arduino libraries (*arduinoFFT*[5]). The demodulation considers the following parameters:

- Sampling frequency (f_S): 40 Hz.
- Number of samples (N_S): 32.

The first parameter (f_S) is determined by the color sensor sampling rate. The second parameter (N_S) is set to 32[6]. Both parameters set the resolution of the FFT, which defines the column *"FFT Frequency (Rx)"* of Table 4 as the best match to the transmitted frequencies. Overall, our transmitter and receiver designs allow us to build a novel short-range wireless communication system, outlined in the next section.

To successfully decode a symbol (instruction) from the received signal, the demodulation process analyzes the frequencies of interest: 5 Hz, 6.25 Hz and 10 Hz, and selects the one with the highest power. However, using the highest spectral energy as the only criterion for decoding a symbol could lead to errors due to ambient light noise. Therefore, we set two conditions for a symbol to be successfully decoded. First, we set a minimum threshold for the spectral power of the highest frequency. Second, the power ratio between the highest and the second highest symbol frequencies needs to be higher than a threshold. Both thresholds are found empirically during experimentation. Figure 12 shows samples of the three symbols received by the CS.

[5]arduinoFFT: https://github.com/kosme/arduinoFFT/tree/master
[6]N_S must be a power of two for the *ArduinoFFT* implementation.

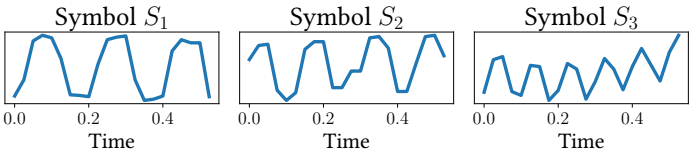

Fig. 12. Samples of the received symbols S_1, S_2 and S_3, corresponding to 5 Hz, 6.67 Hz, and 10 Hz, respectively.

3.3 Edge-Light: a full-duplex transceiver

Based on the previous sections, we implement a full-duplex wireless link based on the transmitter and receiver designs, and Figure 13a shows a schematic description of the Edge-Light transceiver. The goal of this transceiver is to communicate wirelessly over a short distance using ambient light as the source of illumination for the LSC. Compared to all prior studies, *the key novelty of Edge-Light is that the communication is lateral to the propagation direction of ambient light.*

A 3D-printed structure holds the microcontroller, transmitter, and receiver. The transmitter includes three layers –LC, LSC, retro-reflector–, and radiates the modulated beam of light throughout the 360°. Additionally, since the aim is to use different types of ambient light with different intensities, the Arduino implements a calibration function to avoid saturation of the receiver's color sensor, sampling it and tuning its gain.

To showcase our mobile Edge-Light implementation and ease its assessment, we use the *Maqueen PLUS v2*[7], which is an STEAM educational robot controlled by a *micro:bit*[8] microcontroller, and place an Edge-Light transceiver on top of the robot. Thus, the robot is able to send and receive commands from other robots.

The robot sends commands using the symbols' frequencies, switching to a different frequency to change the command. We set some conditions that limit these frequencies. First, the color sensor sampling interval must be higher than 24 ms. Second, to avoid using more than one timer, we set an interval of 25 ms (or 40 Hz) to both read the color sensor and change the state of the LC, which limits the highest frequency detected by the FFT to 10 Hz[9]. Furthermore, we discard frequencies below 2.5 Hz to avoid overlapping with slow changes in light intensity, which can be caused by motion (indoors) or variation in weather conditions (outdoors). These constraints combined with the selected FFT size (32 bits) render the frequencies in Table 4.

On the other hand, for the robot to receive a command, the transceiver is constantly trying to decode symbols from the color sensor and sends the result to the robot's controller via a serial port. We leverage the LED panel of the *micro:bit* as a visual aid to show the decoded symbol, so we can validate visually the link. We also use the wheels and engines to assess Edge-Light under motion, as presented in the next section.

4 Evaluation

In this section, we evaluate the performance of Edge-Light under two conditions: standard indoor illumination and sunlight. Our setups include a static and mobile evaluation of the link.

4.1 Indoors: Constant Ceiling light

Indoor environments with human presence usually require around 500 lx of illumination. We test Edge-Light in a working environment using a ceiling light that provides around 450 lx[10].

[7]Maqueen Plus: https://wiki.dfrobot.com/SKU_MBT0021-EN_Maqueen_Plus_STEAM_Programming_Educational_Robot
[8]micro:bit https://microbit.org/
[9]The FFT detects frequencies below 20 Hz. However, by using the same timer for modulation and demodulation, the highest is 10 Hz
[10]The light intensity is measured at the floor level of the room used in the experiments.

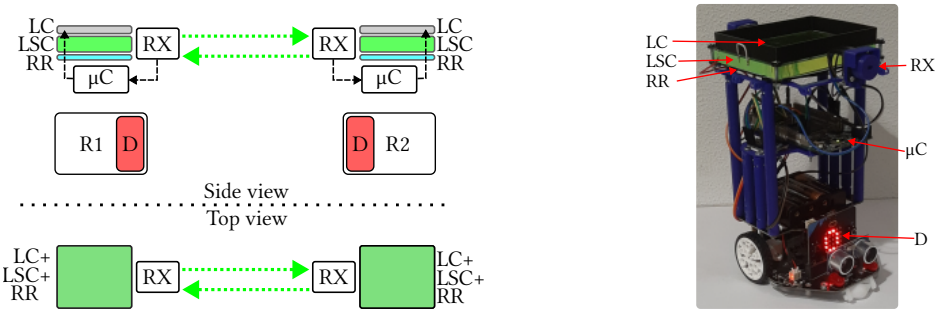

(a) Transeivers system diagram.

(b) Implementation.

Fig. 13. Edge-Light implementation of a full-duplex link. R: robot, D: display.

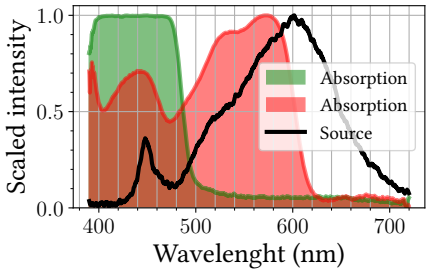

Fig. 14. Spectrum of indoor ambient light. Overlaid are the absorption spectra of the green and red LSC.

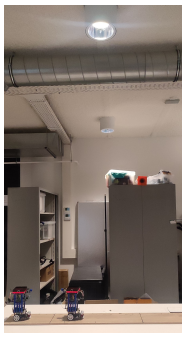

Fig. 15. Setup for indoor experiments.

Lighting is provided by different types of bulbs. Depending on the architectural design, light bulbs provide different radiation patterns and spectra. The radiation patterns do not affect significantly the operation of the LSC, because LSCs are agnostic to the incidence angle of ambient light. The light spectrum may have an impact depending on the technology used to generate white light, but the green and red bands are well within the visible light spectrum, and hence, Edge-Light works under different ambient light conditions, as it is shown later in an outdoor setup.

Given that the ambient light spectra play a role in the emitted band, as mentioned in section 2, the first step of our analysis is to measure the spectrum of the light source. Figure 14 shows this spectrum, which is a typical white light source, noting that its intensity is weak at lower wavelengths (towards the color blue) and stronger at higher wavelengths (towards the color red). Thus, we expect the performance of the red LSC to be better than the green LSC. To analyze the performance of the different emitted bands, the evaluation includes robots with different Edge-Light transmitters: one with a green LSC and one with a red LSC.

The distance between both robots is increased, starting from 15 cm, in steps of 15 cm. At each step, the robots are static and constantly sending one of the 3 symbols. To assess the link, we use the SNR of each symbol's frequency (Table 4) and the symbol success rate (SSR), the percentage of correctly decoded symbols.

4.1.1 Results. Figure 16 present the results, which show a better performance of the red LSC compared to the green LSC, giving a greater SNR and SSR at all distances and for all symbols (frequencies). The results show that

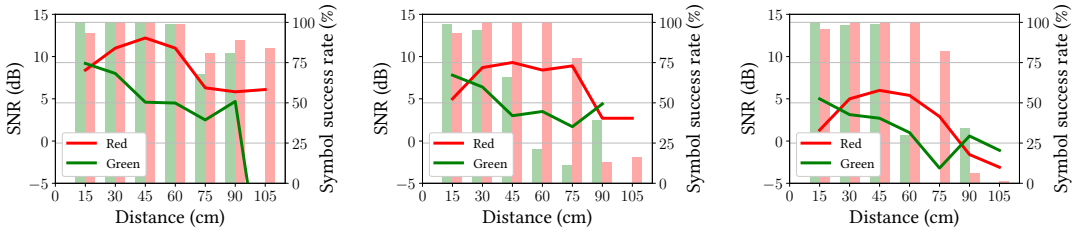

(a) Symbol S_1 (5.0 Hz) (b) Symbol S_2 (6.7 Hz) (c) Symbol S_3 (10.0 Hz)

Fig. 16. SNR (lines) and SSR (bars) for indoor experiments at different distances with static transceivers, red and green LSC.

the SNR decays as the symbol frequency increases. This occurs because as the switching frequency of the LC increases, the contrast between the dark and transparent states reduces. Another feature of the results is the low performance of the S_2 symbol, with a performance similar to the symbol with the fastest frequency, S_3. The reason for this phenomenon is the mismatch between the transmitted frequency and the frequency bin from the FFT, 6.7 Hz and 6.25 Hz, as described in Table 4. The mismatch reduces the link's performance at this particular frequency.

Overall, we note that, indoors, Edge-Light works better with the red LSC because its absorption band matches better with the illumination. Next, we test the system in a mobile setting. From the results, we notice that in the static case an SNR lower than 5 dB drastically reduces the link's performance.

4.2 Variable Incidence Light: The effect of motion

The previous test does not include motion. Under that setup, the intensity and incidence angle of ambient light is constant. In this section, we let the robots communicate while both move in line. The movement of the robots changes their relative position concerning the ceiling illumination, creating a "dynamic" lightning condition with changes in intensity and incidence angles.

The distance between the robots is set to 30 cm because based on the previous results that distance gives a reliable SSR for all symbols with both LSCs, green and red. We set the following conditions for the movement: a speed of ~6 cm/s for both robots and they move for ~25 s covering a distance of ~150 cm.

For the experiments, we placed the robots under the same ceiling light as before and gave both robots a trigger signal to start the motors. At all times, both robots transmit and decode information, transmitting only one symbol per experiment. Each experiment is repeated twice per symbol to get one hundred samples per symbol.

4.2.1 Results. Mobility reduces the performance of Edge-Light, more specifically the SNR and the SSR of the green LSC. Figure 17 shows the SNR and SRR for both LSC transceivers. Next, we describe the reasons why mobility reduces the system's performance.

SNR under dynamic conditions. For the static conditions under indoor illumination, all parameters are fixed, including the intensity and incidence angle of light. Therefore, the signal is constant with a periodic oscillation at the transmitted frequency. However, under dynamic conditions, the signal becomes highly variable as shown in Figure 18a. Due to this variability, the FFT leads to a noisy spectrum for the green LSC, as depicted in Figure 18b.

The mobility noise comes from two sources. First, moving towards/away from the light source creates changes in intensity. Second, the mechanical vibration caused by the robots' motion introduces small misalignments that lead to changes in intensity. Regardless of the added noise addition, the red LSC maintains a strong spectral response, as shown in Figure 18b.

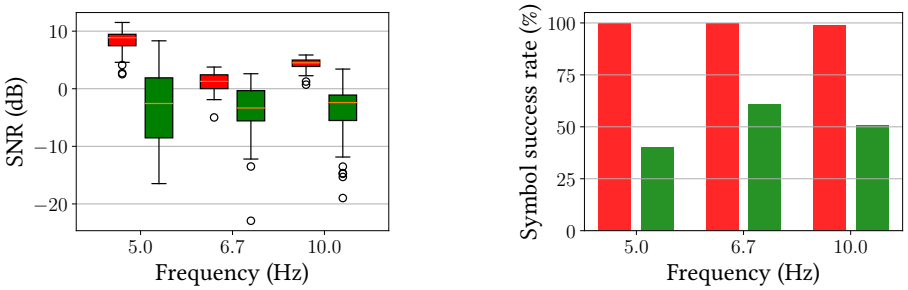

(a) SNR (b) SSR

Fig. 17. SNR and SSR for indoor experiments with transceivers in motion.

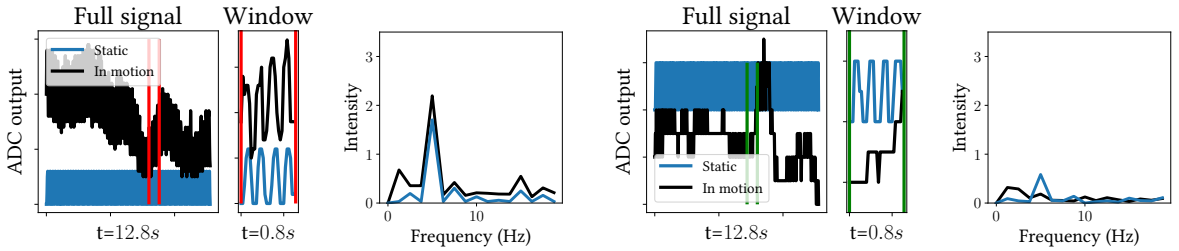

(a) Time domain (b) Frequency domain (c) Time domain (d) Frequency domain

Fig. 18. Time and frequency signals comparison between the *static* and *in motion* cases for the symbol S_1 (5 Hz) for red-LSC Edge-Light (a, b) and green-LSC Edge-Light (c, d)

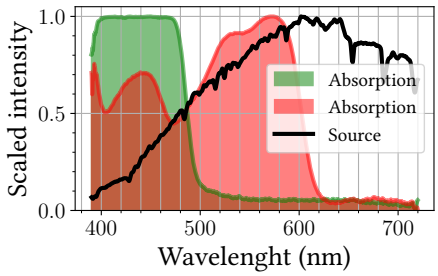

Fig. 19. Sunlight spectrum during the outdoor experiments. Overlaid are the absorption spectra of the green and red LSC.

4.3 Outdoors: variable sunlight intensity

The main idea behind Edge-Light is to create a wireless link that leverages sunlight using LSCs. Therefore, our next experiments assess the system's performance during daylight.

The experiments are performed between 11:00 and 14:00 the same day. During these periods we recorded sunlight intensities larger than 100 klx, 20 times stronger compared to the indoor experiments. Figure 20 depicts a sample deployment outdoors. Another important point is that the spectrum of sunlight differs from the spectrum

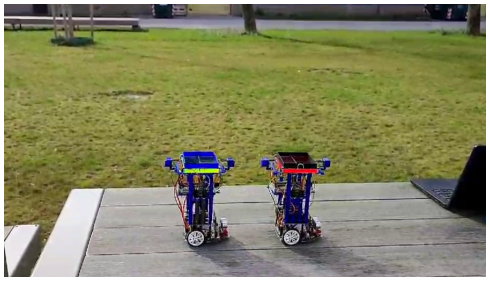

Fig. 20. Outdoors experiment setup.

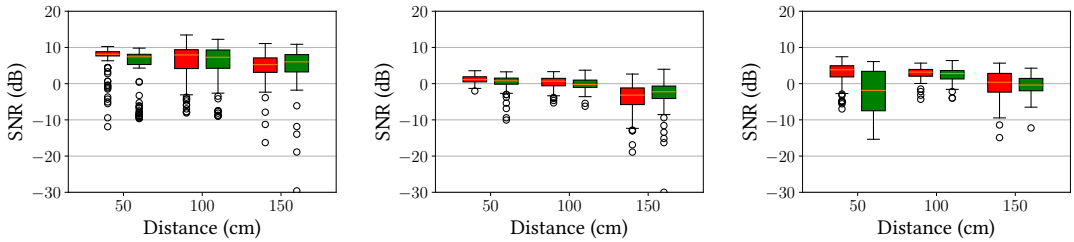

(a) Symbol S_1 (5.0 Hz) (b) Symbol S_2 (6.7 Hz) (c) Symbol S_3 (10.0 Hz)

Fig. 21. SNR for outdoor experiments at different distances with stationary transceivers, red and green LSC.

of indoor lighting, as depicted in Figure 19. Compared to indoor light, sunlight is stronger in the absorption band of the green LSC but still matches better with the band of the red LSC.

Similar to the indoor experiments, each robot is placed at a fixed distance from the other, while they send and receive information simultaneously, without any relative motion between them. Due to the higher light intensity, the calibration function of the CS is important to avoid saturation.

4.3.1 Results. The stronger sunlight intensity boosts the link's performance, as shown in Figure 22. More light reaches the LSC surface, boosting the edge light emission. The range is *almost* doubled, from 50 cm to 100 cm for the green LSC and from 75 cm to 150 cm for the red LSC.

While the range is boosted, sunlight also brings variability issues. This variability can be observed in the higher number of outliers present in the boxplot of the outdoor scenario (Figure 21) compared to the indoor one (Figure 17a). Sunlight variability can occur at a slow pace and high pace. At a slow pace, the changes in intensity are gradual and Edge-Light works well. However, at a high changing pace, we observed errors even at close ranges, as shown in Figure 22c, where the green LSC has a low SSR at 50 cm. During this part of the experiment, the intensity oscillated rapidly –a few times per second– due to a cloudy and windy part of the day where sunlight changed between 80 klx to 50 klx, affecting the decoding performance. Since the red LSC has a stronger signal strength, these variations did not affect the red LSC as much as the green LSC.

The outdoor Edge-Light's experiments show its ability to harness sunlight to create a new type of wireless link. In the next section, we take a step further and use Edge-Light as a communication system for robots.

5 Robot-to-robot communication

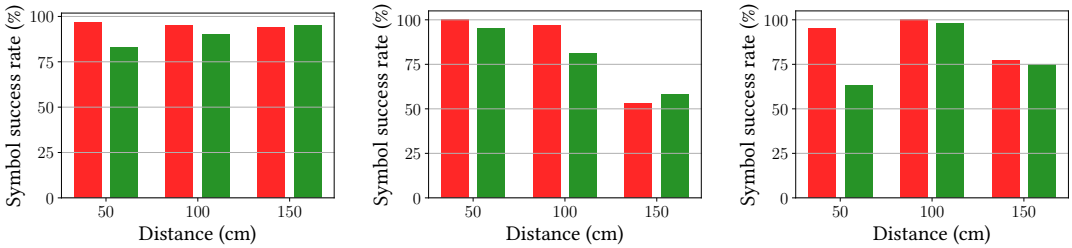

(a) Symbol S_1 (5.0 Hz). (b) Symbol S_2 (6.7 Hz). (c) Symbol S_3 (10.0 Hz).

Fig. 22. SSR for outdoor experiments at different distances with stationary transceivers.

Thus far, the experiments presented rely only on one color sensor, which is facing the other robot directly. This setup limits the mobility of the robots, as they can only move in a straight line. Because the LSC transmitter is omnidirectional, we enhance the Edge-Light receiver by adding 3 extra color sensors at each side of the robot, thus adding the option for the robots to rotate and keep connected.

To attain robot cooperation, we program one robot as the *parent* and the other as the *child*. The robots exchange 3 symbols which translate into 3 instructions: IDLE, MOVE FORWARD, ROTATE 90°, and the logic for executing a task is the following:

(1) The parent detects an IDLE message from the child.
(2) The parent sends a MOVE FORWARD/ROTATE message to the child.
(3) The child detects the MOVE FORWARD/ROTATE message, and sends the same instruction back to the parent, so both robots can start a coordinated movement. After a specific amount of time, the child executes the instruction.
(4) The parent detects the instruction from the child, which acts as an acknowledgment, waits for a specific amount of time and executes the instruction.

In the next section, we use two robots and this set of instructions to carry out two basic tasks: coordinated movement of the two robots and simultaneously pushing a box. The box is too heavy to be pushed by one robot, but it can be pushed by two robots.

5.1 Enabling robots' joint tasks with Edge-Light

In this section, the robots use the 3 instructions (IDLE, MOVE FORWARD and ROTATE) to perform coordinated or collaborative tasks. Similar to the previous section, the robots are placed in different scenarios. Due to the better performance of the red LSC, the experiments are done with that configuration. Additionally, the robot on the right side of all figures in this section is set to be the parent. **These experiments are better appreciated in the videos attached to this submission.**

5.1.1 Indoor scenario: ceiling light. Under a standard ceiling fixture, the robots perform one coordinated task and one collaborative task.

Coordinated task. In this experiment, the parent requests the child to move to a different point and then come back to the starting point. In the video, the oscillation of the LCs is visible while transmitting the messages. Figure 23 shows snapshots of the video. The exact instructions sent by the parent are:

(1) MOVE FORWARD, IDLE
(2) ROTATE, IDLE
(3) ROTATE, IDLE

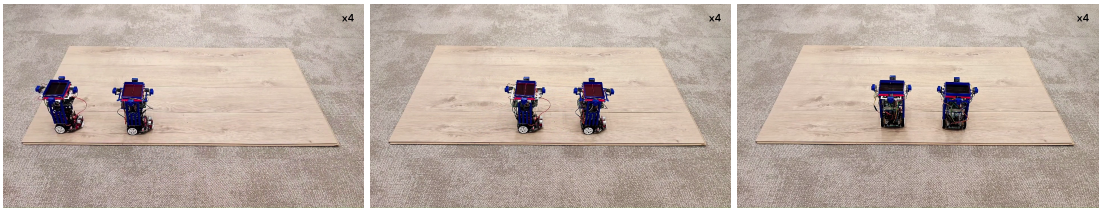

(a) Starting position. (b) MOVE FORWARD, IDLE. (c) ROTATE, IDLE.

Fig. 23. Indoor coordinated task. **The video is attached to this submission.**

(a) Starting position. (b) ROTATE. (c) MOVE FORWARD.

Fig. 24. Unsuccessful individual task. One robot fails to push the carton box. **Video is attached**

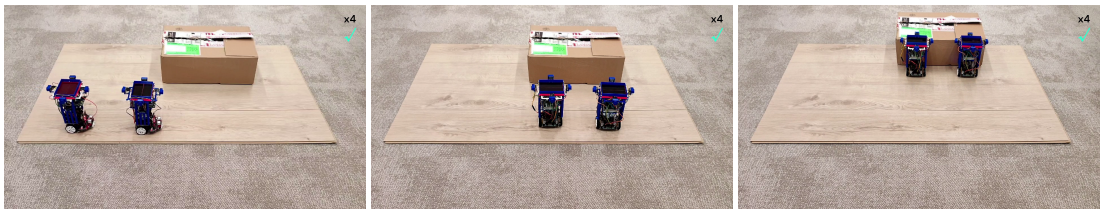

(a) Starting position. (b) ROTATE, IDLE. (c) MOVE FORWARD.

Fig. 25. Successful collaborative task. Two robots push the carton box. **Video is attached**

(4) MOVE FORWARD, IDLE

Both calibrations are repeated for each task.

Collaborative task. Some robot tasks require cooperation. To showcase a sample scenario, we devised a setup where the goal is to push a carton box. First, the parent tries to push the box using the sequence:

(1) MOVE FORWARD, IDLE
(2) ROTATE, IDLE
(3) MOVE FORWARD

However, the engines of one robot are not powerful enough to achieve the task, and after the final step of the task sequence, the box does not move and the robot gets stuck in front of the box (Figure 24c). In a second setup, the parent and child coordinate their moves to push the box successfully, Figure 25c.

5.1.2 Outdoor scenario using sunlight. The communication between moving robots also works under sunlight.

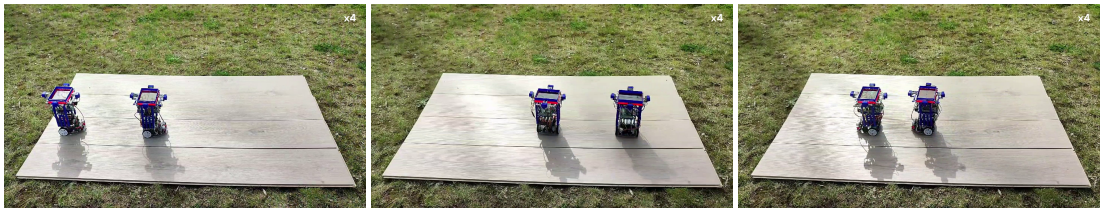

(a) Starting position. (b) ROTATE, IDLE. (c) MOVE FORWARD, IDLE.

Fig. 26. Outdoor coordinated task. **Video is attached**.

Coordinated task The parent is programmed with the same instructions as the indoor coordinated task (MOVE FORWARD, IDLE, ROTATE, IDLE, ROTATE, IDLE, MOVE FORWARD, IDE). The result is a successful in-sync motion and rotation of the parent and the child, as depicted in Figure 26. Regardless of the type of illumination, indoors and constant or outdoors and variable, Edge-Light is able to establish an optical wireless connection between robots to perform joint tasks.

6 Related Work

The analysis of the SoA focuses on visible light communication. VLC aims to complement, not replace, radio-frequency (RF) systems. RF is a mature technology with higher data rates and better power efficiency than VLC, such as BLE. Visible light communication is a young technology with ample room for improvement but exploits a free and empty spectrum.

6.1 Active VLC

The research community has explored the concept of VLC since 2000[27] and the advances in this field have encouraged the development of commercial VLC platforms. *LiFi*, the commercial implementation of VLC, renders a combination of illumination and VLC up to ~10 m, with some companies reportedly attaining data transmission speeds up to 1 Gbps[29], including devices such as dongles and access points to provide full internet connectivity to mobile devices.

The scientific community explores many variations of VLC achieving higher speeds. In one study, a VLC link of 300 Gbps is demonstrated by using elaborated optical methods, such as wavelength-division multiplexing (WMD) and orthogonal polarization channels[12]. On the other hand, lower-end systems which build upon more simple devices attain links of around 100 kbps[9].

Compared to our work, the implementation of Edge-Light requires a minimum amount of energy compared to (Active) VLC, because the latter requires power to generate light and embed information into it, while Edge-Light uses the LSC ability to repurpose light from the environment, such as sunlight.

6.2 Passive VLC

Light is a ubiquitous source: during the day sunlight illuminates outdoor environments and, because humans need light to perform tasks, indoors or at night we use artificial lighting systems. This overall presence of light has inspired researchers to design and create *Passive VLC* systems that reuse ambient light, thus reducing the energy budget. The work in PassiveVLC[34] uses 0.12 µJ energy per bit, while in [9] this parameter is 30 times larger, 1 mJ.

Among the different passive VLC works, we identify 3 main categories. First, we have the *backscattering* passive VLC systems, which work by using a reflective material to guide back to its source while modulating

the reflected light usually using an LC[13, 30, 31, 34]. Second, other systems focus on using LC as *transmissive surface* to modulate ambient light, which is redirected towards the LC using optical devices[5, 8]. Finally, the third category includes systems that implement a *reflective surface* that redirects the light towards the intended receiver[33].

Related to our work, Edge-Light takes inspiration from the backscattering systems because it also uses light that illuminates a surface. However, Edge-Light redirects light to its edges and not back to the source. Also, these backscattering systems do not work using sunlight. Compared to the LC systems, Edge-Light uses the same device to modulate the light reaching the surface of the LSC. The complexity of the third type of system is greater than the implementation of our system.

6.3 LSC applications

The ability of the LSC to absorb a band of light and emit a different band on its edges has been leveraged in several fields. We mention three of the most relevant

6.3.1 Photovoltaics and buildings. The main use of the LSC is in combination with PV cells[23, 24], which are attached to the emitting edges of the LSC to gather light. The size of the LSC panel influences its performance and research in the performance and optimization of large LSC panels[2, 36]. These large LSC panels are used in buildings as part of windows[4, 11, 28, 36, 38] to capture part of the sunlight spectrum, re-emit light in a different optical band and concentrate it directly on the surface of the solar cells attached to the LSC edges. This application has also triggered the development of *smart windows*[18, 26], which adds the feature of controlling the window's opacity while it gathers and concentrates light.

6.3.2 Horticulture. Plants use a specific part of the light spectrum for the photosynthesis process. Thus, small LSCs can be designed to absorb the bands not used by plants and placed on the top of a greenhouse. These LSCs re-emit light in the spectrum bands used for photosynthesis and concentrate it on their edges. This re-emitted light is captured by optical fibers attached to the LSC edges, and guided to plants located at a lower level in the greenhouse, bringing useful light to the deeper levels without using energy to power up devices. A trial of this concept resulted in a 7 % increase in the crop yield for tomatoes, using 24 cm^2 LSC panels and plastic optical fibers[15].

6.3.3 VLC. In optical wireless communications, LSC is an attractive solution as a receiver antenna due to its large FoV. Such an antenna receives light on its surface and emits light on its edges, where a PD is attached[17]. The malleability of acrylic-based LSC allows the creation of different shapes for the receivers, leveraging planar-parabolic shapes to increase the gain[6] or spherical shapes to manufacture almost omnidirectional receivers[21]. Moreover, the ability to absorb specific spectrum bands allows the implementation of a wavelength-selective receiver seamlessly by stacking two LSCs with complementary absorption bands, for instance, one green and one red. The top LSC absorbs only green light, and lets the other bands pass, while the bottom LSC absorbs the red light; creating a two-band receiver in the same area[16].

Compared to our work, we take a different approach to using the LSC as a VLC transmitter instead of a receiver.

7 Discussion

This section presents some limitations of the current system and potential improvements at each stage.

Range between transceivers. The communication range for our current setup is limited to 50 cm indoors, and it almost doubles outdoors but remains below two meters. A way to increase the range is to add an optical component at the edge of the LSC to concentrate the beam into a narrower (longer) shape. A suitable device to achieve this goal is a collimation lens, which can redirect the light and make it horizontal and more focused towards

the receiver. However, implementing this setup increases the alignment constraints between the transmitter and the receiver, which could reduce the system's mobility.

Link's speed. In the current configuration, the link's data rate is limited by the LC speed and the *integration time* of the CS. The LC speed is a physical limiting factor. However, the LC can operate at a *faster mode*, which reduces the contrast between states, thus reducing also the SNR. The previously discussed lens system could improve the SNR and make this *faster mode* readable. Regarding the CS, if the SNR is large enough, the *integration time* could be reduced to 2.4 ms or we can use a faster CS.

Increasing the number of robots. Edge-Light allows lateral communication between robots and our experiments show how two robots (one parent, one child) communicate using one of the four CS on each side. To increase the number of robots sharing commands simultaneously, we need to set the initial conditions of the parent's location, i.e., if the parent is between two children, the children should read the corresponding CS. The parent/child communication logic must be upgraded because the parent needs to handle receiving symbols from multiple CS, and the acknowledgment and waiting time to execute must be synchronized among more robots. The current hardware implementation of our robot-to-robot communication allows the parent to communicate with a maximum of four children simultaneously. Another possibility is to leverage the malleability of the LSC, which is basically an acrylic, to create transceivers with different shapes, like circular or hexagonal, and add more CSs. Such a setup could enable lateral communication in more directions, such as diagonal.

Different light sources. During our experiments, we used two different light sources: an indoor ceiling light and sunlight. Nonetheless, different artificial light sources have different spectra and refresh rates. Regarding the light source spectrum, a previous spectral analysis of the ambient light is necessary to select the appropriate LSC, which can be commercially available or custom-made in a research facility. The current implementation of Edge-Light uses frequencies below 10 Hz and the usual refresh rates of LED bulbs are higher than 100 Hz, thus we notice no impact in our current implementation. If the hardware allows increasing the transmitter and receiver's frequencies, they must avoid being close to the flickering rate of LED light bulbs.

FFT computation. The implementation of the FFT uses the *arduinoFFT* library with 32 samples per FFT window. With the current sampling period, 25 ms, we found that the number of samples is enough to decode the symbols, regardless of the mismatch for the third symbol, in less than one second. Increasing the number of samples leads to a finer frequency resolution at the cost of more time to capture the signal and compute the FFT.

Multiple transmitters, single receiver. One key feature of the LSC is that the material sets the output spectrum at the edges. In our implementation, we use red and green LSCs, with minimum overlap between the output spectra. Our receiver, based on a CS, is able to differentiate the spectrum by filtering the incoming light into three color channels. One open possibility is to combine multiple transmitters with different color outputs close to each other and in the range of a single receiver. In this way, a single CS can read its red and green channels independently and decode each channel, effectively doubling the speed of the link. However, a careful analysis of the spectra and a CS calibration should be implemented to reduce the effect of the spectrum overlap.

8 Conclusions

In this work, we propose a novel passive VLC transmitter which can work using ceiling lighting and, most significantly, sunlight. Our design is based on an LSC, a material with the capacity to absorb light from the top, redirect it and concentrate it laterally. The full transmitter design incorporates LCs to modulate the incoming light on top, thus modulating the light emitted from the edges. By combining it with an appropriate receiver, in this work a color sensor, we implement a transceiver for a full-duplex optical wireless link. Furthermore, we realize robot-to-robot communication using the Edge-Light transceiver, allowing robots to coordinate collaborative tasks using a sunlight-based wireless connection. Overall, our work demonstrates a new approach in LSC applications and the potential of our transceiver to create a low-power passive VLC link.

Acknowledgments

This work has been funded by the Dutch Research Council (NWO) with a TOP-Grant with project number 612.001.854. The authors would like to thank the Research Experience for Peruvian Undergraduates (REPU) program for facilitating the collaboration with the second author.

References

[1] Ataberk Aksoy, Ömer Yıldız, and Sait Eser Karlık. 2024. Comparative Analysis of End Device and Field Test Device Measurements for RSSI, SNR and SF Performance Parameters in an Indoor LoRaWAN Network. *Wireless Personal Communications* 134, 1 (2024), 339–360.

[2] N. Aste, L.C. Tagliabue, C. Del Pero, D. Testa, and R. Fusco. 2015. Performance analysis of a large-area luminescent solar concentrator module. *Renewable Energy* 76 (2015), 330–337. https://doi.org/10.1016/j.renene.2014.11.026

[3] Haley C. Bauser, Colton R. Bukowsky, Megan Phelan, William Weigand, David R. Needell, Zachary C. Holman, and Harry A. Atwater. 2020. Photonic Crystal Waveguides for >90% Light Trapping Efficiency in Luminescent Solar Concentrators. *ACS Photonics* 7, 8 (2020), 2122–2131. https://doi.org/10.1021/acsphotonics.0c00593 arXiv:https://doi.org/10.1021/acsphotonics.0c00593

[4] Matthew R. Bergren, Nikolay S. Makarov, Karthik Ramasamy, Aaron Jackson, Rob Guglielmetti, and Hunter McDaniel. 2018. High-Performance CuInS2 Quantum Dot Laminated Glass Luminescent Solar Concentrators for Windows. *ACS Energy Letters* 3, 3 (2018), 520–525. https://doi.org/10.1021/acsenergylett.7b01346 arXiv:https://doi.org/10.1021/acsenergylett.7b01346

[5] Rens Bloom, Marco Zúñiga Zamalloa, and Chaitra Pai. 2019. LuxLink: creating a wireless link from ambient light. In *Proceedings of the 17th Conference on Embedded Networked Sensor Systems* (New York, New York) *(SenSys '19)*. Association for Computing Machinery, New York, NY, USA, 166–178. https://doi.org/10.1145/3356250.3360021

[6] Yurong Dong, Meng Shi, Xilu Yang, Pan Zeng, Junyi Gong, Sunming Zheng, Mengjie Zhang, Rongqing Liang, Qiongrong Ou, Nan Chi, and Shuyu Zhang. 2017. Nanopatterned luminescent concentrators for visible light communications. *Opt. Express* 25, 18 (Sep 2017), 21926–21934. https://doi.org/10.1364/OE.25.021926

[7] Seyed Keyarash Ghiasi, Vivian Dsouza, Koen Langendoen, and Marco Zuniga. 2023. SpectraLux: Towards Exploiting the Full Spectrum with Passive VLC. In *Proceedings of the 22nd International Conference on Information Processing in Sensor Networks* (San Antonio, TX, USA) *(IPSN '23)*. Association for Computing Machinery, New York, NY, USA, 274–287. https://doi.org/10.1145/3583120.3586966

[8] Seyed Keyarash Ghiasi, Marco A. Zúñiga Zamalloa, and Koen Langendoen. 2021. A principled design for passive light communication. In *Proceedings of the 27th Annual International Conference on Mobile Computing and Networking* (New Orleans, Louisiana) *(MobiCom '21)*. Association for Computing Machinery, New York, NY, USA, 121–133. https://doi.org/10.1145/3447993.3448629

[9] Borja Genoves Guzman, Muhammad Sarmad Mir, Dayrene Frometa Fonseca, Ander Galisteo, Qing Wang, and Domenico Giustiniano. 2023. Prototyping Visible Light Communication for the Internet of Things Using OpenVLC. *IEEE Communications Magazine* 61, 5 (2023), 122–128. https://doi.org/10.1109/MCOM.001.2200642

[10] Alberto Jiménez-Solano, José-Maria Delgado-Sánchez, Mauricio E Calvo, José M Miranda-Muñoz, Gabriel Lozano, Diego Sancho, Emilio Sánchez-Cortezón, and Hernán Míguez. 2015. Design and realization of transparent solar modules based on luminescent solar concentrators integrating nanostructured photonic crystals. *Prog. Photovolt.* 23, 12 (Dec. 2015), 1785–1792.

[11] A. Kerrouche, D.A. Hardy, D. Ross, and B.S. Richards. 2014. Luminescent solar concentrators: From experimental validation of 3D ray-tracing simulations to coloured stained-glass windows for BIPV. *Solar Energy Materials and Solar Cells* 122 (2014), 99–106. https://doi.org/10.1016/j.solmat.2013.11.026

[12] Chung-Yi Li, Hai-Han Lu, Wen-Shing Tsai, Chao-Yu Feng, Cing-Ru Chou, Yi-Hao Chen, and Agustina Nainggolan. 2020. White-lighting and WDM-VLC system using transmission gratings and an engineered diffuser. *Opt. Lett.* 45, 22 (Nov 2020), 6206–6209. https://doi.org/10.1364/OL.409843

[13] Jiangtao Li, Angli Liu, Guobin Shen, Liqun Li, Chao Sun, and Feng Zhao. 2015. Retro-VLC: Enabling Battery-free Duplex Visible Light Communication for Mobile and IoT Applications. In *Proceedings of the 16th International Workshop on Mobile Computing Systems and Applications* (Santa Fe, New Mexico, USA) *(HotMobile '15)*. Association for Computing Machinery, New York, NY, USA, 21–26. https://doi.org/10.1145/2699343.2699354

[14] Guiju Liu, Raffaello Mazzaro, Changchun Sun, Yuanming Zhang, Yiqian Wang, Haiguang Zhao, Guangting Han, and Alberto Vomiero. 2020. Role of refractive index in highly efficient laminated luminescent solar concentrators. *Nano Energy* 70 (2020), 104470. https://doi.org/10.1016/j.nanoen.2020.104470

[15] Nikolay S. Makarov, Karthik Ramasamy, Aaron Jackson, Andres Velarde, Chloe Castaneda, Nic Archuleta, Damon Hebert, Matthew R. Bergren, and Hunter McDaniel. 2019. Fiber-Coupled Luminescent Concentrators for Medical Diagnostics, Agriculture, and Telecommunications. *ACS Nano* 13, 8 (2019), 9112–9121. https://doi.org/10.1021/acsnano.9b03335 arXiv:https://doi.org/10.1021/acsnano.9b03335 PMID: 31291097.

[16] Pavlos P. Manousiadis, Hyunchae Chun, Sujan Rajbhandari, Dimali A. Vithanage, Rahmat Mulyawan, Grahame Faulkner, Harald Haas, Dominic C. O'Brien, Steve Collins, Graham A. Turnbull, and Ifor D. W. Samuel. 2020. Optical Antennas for Wavelength

Division Multiplexing in Visible Light Communications beyond the Étendue Limit. *Advanced Optical Materials* 8, 4 (2020), 1901139. https://doi.org/10.1002/adom.201901139 arXiv:https://onlinelibrary.wiley.com/doi/pdf/10.1002/adom.201901139

[17] Pavlos P. Manousiadis, Sujan Rajbhandari, Rahmat Mulyawan, Dimali A. Vithanage, Hyunchae Chun, Grahame Faulkner, Dominic C. O'Brien, Graham A. Turnbull, Stephen Collins, and Ifor D.W. Samuel. 2016. Wide field-of-view fluorescent antenna for visible light communications beyond the étendue limit. *Optica* 3, 7 (Jul 2016), 702–706. https://doi.org/10.1364/OPTICA.3.000702

[18] Fahad Mateen, Mumtaz Ali, Heemuk Oh, and Sung-Kyu Hong. 2019. Nitrogen-doped carbon quantum dot based luminescent solar concentrator coupled with polymer dispersed liquid crystal device for smart management of solar spectrum. *Solar Energy* 178 (2019), 48–55. https://doi.org/10.1016/j.solener.2018.12.013

[19] Barry McKenna and Rachel C. Evans. 2017. Towards Efficient Spectral Converters through Materials Design for Luminescent Solar Devices. *Advanced Materials* 29, 28 (2017), 1606491. https://doi.org/10.1002/adma.201606491 arXiv:https://onlinelibrary.wiley.com/doi/pdf/10.1002/adma.201606491

[20] Ioannis Papakonstantinou, Mark Portnoi, and Michael G. Debije. 2021. The Hidden Potential of Luminescent Solar Concentrators. *Advanced Energy Materials* 11, 3 (2021), 2002883. https://doi.org/10.1002/aenm.202002883 arXiv:https://onlinelibrary.wiley.com/doi/pdf/10.1002/aenm.202002883

[21] T. Peyronel, K. J. Quirk, S. C. Wang, and T. G. Tiecke. 2016. Luminescent detector for free-space optical communication. *Optica* 3, 7 (Jul 2016), 787–792. https://doi.org/10.1364/OPTICA.3.000787

[22] Loredana Protesescu, Sergii Yakunin, Maryna I. Bodnarchuk, Franziska Krieg, Riccarda Caputo, Christopher H. Hendon, Ruo Xi Yang, Aron Walsh, and Maksym V. Kovalenko. 2015. Nanocrystals of Cesium Lead Halide Perovskites (CsPbX3, X = Cl, Br, and I): Novel Optoelectronic Materials Showing Bright Emission with Wide Color Gamut. *Nano Letters* 15, 6 (2015), 3692–3696. https://doi.org/10.1021/nl5048779 arXiv:https://doi.org/10.1021/nl5048779 PMID: 25633588.

[23] Mehran Rafiee, Subhash Chandra, Hind Ahmed, and Sarah J. McCormack. 2019. An overview of various configurations of Luminescent Solar Concentrators for photovoltaic applications. *Optical Materials* 91 (2019), 212–227. https://doi.org/10.1016/j.optmat.2019.01.007

[24] Bryce S. Richards and Ian A. Howard. 2023. Luminescent solar concentrators for building integrated photovoltaics: opportunities and challenges. *Energy Environ. Sci.* 16 (2023), 3214–3239. Issue 8. https://doi.org/10.1039/D3EE00331K

[25] Marika Savarese, Anna Aliberti, Ilaria De Santo, Edmondo Battista, Filippo Causa, Paolo A. Netti, and Nadia Rega. 2012. Fluorescence Lifetimes and Quantum Yields of Rhodamine Derivatives: New Insights from Theory and Experiment. *The Journal of Physical Chemistry A* 116, 28 (2012), 7491–7497. https://doi.org/10.1021/jp3021485 arXiv:https://doi.org/10.1021/jp3021485 PMID: 22667332.

[26] Jeroen A. H. P. Sol, Gilles H. Timmermans, Abraham J. van Breugel, Albertus P. H. J. Schenning, and Michael G. Debije. 2018. Multistate Luminescent Solar Concentrator "Smart" Windows. *Advanced Energy Materials* 8, 12 (2018). https://doi.org/10.1002/aenm.201702922 Cited by: 80; All Open Access, Green Open Access, Hybrid Gold Open Access.

[27] Y. Tanaka, S. Haruyama, and M. Nakagawa. 2000. Wireless optical transmissions with white colored LED for wireless home links. In *11th IEEE International Symposium on Personal Indoor and Mobile Radio Communications. PIMRC 2000. Proceedings (Cat. No.00TH8525)*, Vol. 2. 1325–1329 vol.2. https://doi.org/10.1109/PIMRC.2000.881634

[28] Mikhail Vasiliev, Kamal Alameh, Mohsin Ali Badshah, Seok-Min Kim, and Mohammad Nur-E-Alam. 2018. Semi-Transparent Energy-Harvesting Solar Concentrator Windows Employing Infrared Transmission-Enhanced Glass and Large-Area Microstructured Diffractive Elements. *Photonics* 5, 3 (2018). https://doi.org/10.3390/photonics5030025

[29] Velmenni. 2023. Li-Fi Dongle and Access Point. https://www.velmenni.com/lifi-dongle-access-points

[30] Purui Wang, Lilei Feng, Guojun Chen, Chenren Xu, Yue Wu, Kenuo Xu, Guobin Shen, Kuntai Du, Gang Huang, and Xuanzhe Liu. 2020. Renovating road signs for infrastructure-to-vehicle networking: a visible light backscatter communication and networking approach. In *Proceedings of the 26th Annual International Conference on Mobile Computing and Networking* (London, United Kingdom) *(MobiCom '20)*. Association for Computing Machinery, New York, NY, USA, Article 6, 13 pages. https://doi.org/10.1145/3372224.3380883

[31] Yue Wu, Purui Wang, Kenuo Xu, Lilei Feng, and Chenren Xu. 2020. Turboboosting Visible Light Backscatter Communication. In *Proceedings of the Annual Conference of the ACM Special Interest Group on Data Communication on the Applications, Technologies, Architectures, and Protocols for Computer Communication* (Virtual Event, USA) *(SIGCOMM '20)*. Association for Computing Machinery, New York, NY, USA, 186–197. https://doi.org/10.1145/3387514.3406229

[32] Kenuo Xu, Chen Gong, Bo Liang, Yue Wu, Boya Di, Lingyang Song, and Chenren Xu. 2023. Low-Latency Visible Light Backscatter Networking with RetroMUMIMO. In *Proceedings of the 20th ACM Conference on Embedded Networked Sensor Systems* (<conf-loc>, <city>Boston</city>, <state>Massachusetts</state>, </conf-loc>) *(SenSys '22)*. Association for Computing Machinery, New York, NY, USA, 448–461. https://doi.org/10.1145/3560905.3568507

[33] Talia Xu, Miguel Chávez Tapia, and Marco Zúñiga. 2022. Exploiting Digital Micro-Mirror Devices for Ambient Light Communication. In *19th USENIX Symposium on Networked Systems Design and Implementation (NSDI 22)*. USENIX Association, Renton, WA, 387–400. https://www.usenix.org/conference/nsdi22/presentation/xu-talia

[34] Xieyang Xu, Yang Shen, Junrui Yang, Chenren Xu, Guobin Shen, Guojun Chen, and Yunzhe Ni. 2017. PassiveVLC: Enabling Practical Visible Light Backscatter Communication for Battery-free IoT Applications. In *Proceedings of the 23rd Annual International Conference on Mobile Computing and Networking* (Snowbird, Utah, USA) *(MobiCom '17)*. Association for Computing Machinery, New York, NY, USA,

180–192. https://doi.org/10.1145/3117811.3117843

[35] Zhice Yang, Zeyu Wang, Jiansong Zhang, Chenyu Huang, and Qian Zhang. 2015. Wearables Can Afford: Light-weight Indoor Positioning with Visible Light. In *Proceedings of the 13th Annual International Conference on Mobile Systems, Applications, and Services* (Florence, Italy) *(MobiSys '15)*. Association for Computing Machinery, New York, NY, USA, 317–330. https://doi.org/10.1145/2742647.2742648

[36] Jun Zhang, Mengjiao Wang, Yi Zhang, Hao He, Wei Xie, Mengmeng Yang, Jianjun Ding, Jun Bao, Song Sun, and Chen Gao. 2015. Optimization of large-size glass laminated luminescent solar concentrators. *Solar Energy* 117 (2015), 260–267. https://doi.org/10.1016/j.solener.2015.05.004

[37] Haiguang Zhao. 2019. Refractive index dependent optical property of carbon dots integrated luminescent solar concentrators. *Journal of Luminescence* 211 (2019), 150–156. https://doi.org/10.1016/j.jlumin.2019.03.039

[38] Yimu Zhao and Richard R. Lunt. 2013. Transparent Luminescent Solar Concentrators for Large-Area Solar Windows Enabled by Massive Stokes-Shift Nanocluster Phosphors. *Advanced Energy Materials* 3, 9 (2013), 1143–1148. https://doi.org/10.1002/aenm.201300173